

Analytic evaluation of non-adiabatic couplings within the complex absorbing potential equation-of-motion coupled-cluster method

Koushik Chatterjee,^{*,†} Zsuzsanna Koczor-Benda,[‡] Xintian Feng,[¶] Anna I.
Krylov,[§] and Thomas-C. Jagau[†]

[†]*Department of Chemistry, KU Leuven, Celestijnenlaan 200F, B-3001 Leuven, Belgium*

[‡]*Department of Chemistry, University of Warwick, Coventry, CV4 7AL, UK*

[¶]*Q-Chem, Inc., 6601 Owens Drive, Suite 240, Pleasanton, CA 94588, USA*

[§]*Department of Chemistry, University of Southern California, Los Angeles, CA 90089,
USA*

E-mail: koushikchatterjee7@gmail.com

Abstract

We present the theory for the evaluation of non-adiabatic couplings (NACs) involving resonance states within the complex absorbing potential equation-of-motion coupled-cluster (CAP-EOM-CC) framework implemented within the singles and doubles approximation. Resonance states are embedded in the continuum and undergo rapid decay through autodetachment. In addition, nuclear motions can facilitate transitions between different resonances and between resonances and bound states. These non-adiabatic transitions affect the chemical fate of resonances and have distinct spectroscopic signatures. The NAC vector is a central quantity needed to model such effects.

In the CAP-EOM-CC framework, resonance states are treated on the same footing as bound states. Using the example of fumaronitrile, which supports a bound radical anion and several anionic resonances, we analyze the non-adiabatic coupling between bound states and pseudocontinuum states, between bound states and resonances and between two resonances. We find that the NAC between a bound state and a resonance is nearly independent of the CAP strength and thus straightforward to evaluate whereas the NAC between two resonance states or between a bound state and a pseudocontinuum state is more difficult to evaluate.

1 Introduction

The Born-Oppenheimer (BO) separation of nuclear and electronic motion is a cornerstone of quantum chemistry and molecular physics of bound states and gives rise to the concept of electronic states and potential energy surfaces (PES).¹⁻⁷ It relies on the fact that the nuclei are significantly heavier and move slower than electrons. In many circumstances, one can invoke an adiabatic approximation, often referred to as the BO approximation, in which the couplings between different electronic states are neglected and nuclear motions on each PES are entirely independent from each other. This means that the electrons follow the nuclei instantly and the electronic state never changes. The BO approximation is in particular appropriate for the ground electronic state, which is usually well separated from the electronically excited states so that non-adiabatic interactions are highly improbable.

However, the BO approximation breaks down when two electronic states become close to each other, for example, near a conical intersection. Here, states are coupled by the kinetic energy operator, which induces transitions between them. Physically, this coupling results from the dependence of the electronic wave functions on the nuclear coordinates. Mathematically, the coupling comprises two terms:⁶⁻⁹ One term is a vector coupling involving the first derivative of the electronic wave functions, which is termed the non-adiabatic coupling (NAC) vector, whereas the other term is a scalar coupling involving the second derivative of

the electronic wave functions. This second term is related to the diagonal Born-Oppenheimer correction.

NAC is thus a central quantity needed to describe non-adiabatic interactions between electronic states mediated by nuclear motion. These interactions give rise to non-adiabatic transitions, intensity borrowing, and vibronic effects. Non-adiabatic transitions result in radiationless relaxation, which is important in photochemistry.²⁻⁶

For bound electronic states that are stable with respect to electron loss the computation of NACs is possible with a variety of quantum-chemical methods including time-dependent density functional theory,¹⁰⁻¹³ multiconfigurational self-consistent field approaches,^{14,15} multireference configuration interaction,^{14,16,17} and equation-of-motion coupled-cluster theory.¹⁸⁻²²

The situation is different for electronic resonances that decay through autodetachment. There is, however, substantial spectroscopic evidence that NAC plays a critical role for these metastable states as well. Recent examples include anionic resonances in pyrrole,^{23,24} para-benzoquinone,^{25,26} chlorobenzene,²⁷ and hexachlorobenzene.²⁸ The evaluation of NACs with quantum-chemical methods for such systems has so far only been possible by approximating resonances as bound states and neglecting their decay.

However, this is not a good approximation because resonances are coupled to the continuum and cannot be associated with discrete states in Hermitian quantum mechanics.²⁹⁻³¹ Rather, they manifest themselves through an increased density of continuum states. In this framework, a treatment of resonances in terms of scattering theory is possible.^{32,33} In contrast, in non-Hermitian quantum mechanics it is possible to describe a resonance by a discrete state with complex energy whose real part is interpreted similarly to the energy of a bound state while the imaginary part corresponds to the decay width, that is, the inverse of the state's lifetime. This result can be reached using two different approaches—the formalism by Gamov and Siegert,^{34,35} where the resonance is an adiabatic state, and the formalism by Feshbach and Fano,³⁶⁻³⁹ where the resonance is treated as a bound state diabatically coupled to the continuum. In the former case, the decay width is a local function of the

nuclear coordinates, whereas in the latter case it is a non-local quantity.

Nuclear motion on resonance PESs and NAC between electronic resonances have been analyzed by several authors.^{40–52} In particular, a linear vibronic coupling model for resonance-resonance interaction has been devised.⁴⁵ Importantly, the BO approximation cannot be applied to resonances without modifications because there is always exact energetic degeneracy between a resonance state and the continuum in which it is embedded. Most of the available theoretical treatments are based on the Feshbach formalism and scattering theory. This approach leads to energy-dependent non-local terms in the resonance potential energy surfaces as well as in the coupling matrix elements.^{44,45,47,53} The non-local treatment is highly accurate but its high computational cost and the intricate nature of the coupling matrix elements make it difficult to apply to more than very few nuclear degrees of freedom. Resonances in polyatomic molecules can thus only be treated within models with reduced dimensionality.

A significant simplification is achieved by the local approximation, which results in an effective complex-valued potential for the motion of the nuclei called the boomerang model.^{54–57} Coupling between resonances can be treated within this model as well.⁴⁷ However, a general problem of the Feshbach formalism is the definition of the resonance state. Especially for molecular temporary anions, there is no easy way to separate the resonance from the embedding continuum. Consequently, the boomerang model and treatments of NAC based on it have not been combined with state-of-the-art quantum chemistry methods so far.

It thus appears worthwhile to use the Siegert formalism for the treatment of NACs involving resonance states. Within this approach, temporary anions of polyatomic molecules can be treated more easily using quantum chemistry methods. For example, crossing seams between anionic resonance states have been computed and analyzed using Siegert energies.^{48,51}

In this article, we present the theory for the analytic evaluation of NACs within the complex absorbing potential equation-of-motion coupled-cluster framework (CAP-EOM-CC).^{58–60}

Our approach is based on analytic gradient theory for CAP methods;^{61,62} the NAC elements are computed following the summed-state approach of Tajti and Szalay.²⁰ An important advantage of CAP-EOM-CC for the study of anionic resonances is that the ground and excited states of the neutral molecule and the bound and resonance states of the corresponding anion are treated on same footing. CAP-EOM-CC analytic gradients have been used to compute adiabatic electron affinities of temporary anions,⁶² to locate minimum-energy crossing points between anionic and neutral PESs,⁶³ to characterize exceptional points,⁵¹ and most recently to investigate the electron-energy loss spectrum of pyrrole.²³

The article is organized as follows. In Section 2 we present the theory of NACs involving resonance states and their evaluation within CAP-EOM-CC theory and in Section 3 we describe our implementation. To illustrate complex-valued NACs obtained from these calculations, we use anionic states of fumaronitrile as an example. The computational details are outlined in Section 4 and the results are discussed in Section 5. Our concluding remarks are given in Section 6.

2 Theory

2.1 Non-adiabatic coupling between bound electronic states

We begin with a brief description of NAC between bound electronic states within the context of the BO separation of variables.⁶ The time-independent Schrödinger equation of a molecule can be written as

$$\hat{H} |\Psi(r, R)\rangle = \mathcal{E} |\Psi(r, R)\rangle \tag{1}$$

where R and r denote nuclear and electronic coordinates, respectively. The total Hamiltonian $\hat{H}(r, R) = \hat{T}_n(R) + \hat{H}^{el}(r, R)$ consists of the electronic Hamiltonian \hat{H}^{el} and the nuclear kinetic energy operator \hat{T}_n . The total wave function $\Psi_T(r, R)$ for a vibronic state T can be expressed

using a sum over products of nuclear and electronic wave functions,

$$|\Psi_T(r, R)\rangle = \sum_I |\Phi_I(r; R)\rangle \xi_I^T(R) . \quad (2)$$

Within the BO separation, the electronic wave functions $|\Phi_I(r; R)\rangle$ are obtained by solving the electronic Schrödinger equation at fixed nuclear positions,

$$\hat{H}^{el} |\Phi_I(r; R)\rangle = E_I(R) |\Phi_I(r; R)\rangle \quad (3)$$

with E_I as electronic energy of adiabatic state I .

The equations that determine the nuclear wave functions $\xi_I^T(R)$ are obtained by plugging Eq. (2) into Eq. (1)

$$\left[\hat{T}_n(R) + \hat{H}^{el}(r, R) \right] \sum_I |\Phi_I(r; R)\rangle \xi_I^T(R) = \mathcal{E}^T \sum_I |\Phi_I(r; R)\rangle \xi_I^T(R) \quad (4)$$

and projection of the Schrödinger equation onto an electronic state $\langle \Phi_J |$. This yields

$$\left[\hat{T}_n + E_J(R) \right] |\xi_J^T(R)\rangle + \sum_I \hat{\Lambda}_{JI} |\xi_I^T(R)\rangle = \mathcal{E}^T |\xi_J^T(R)\rangle . \quad (5)$$

The first term in Eq. (5) describes nuclear motion on an isolated PES $E_J(R)$, while $\hat{\Lambda}_{JI}$ ($I \neq J$) is the NAC between states J and I . Within the BO approximation, $\hat{\Lambda}_{JI}$ is neglected resulting in the separation of electronic and nuclear degrees of freedom. However, to describe non-adiabatic transitions between electronic states, this term needs to be considered. The coupling matrix element is given by

$$\hat{\Lambda}_{JI} = \sum_{\alpha} \frac{1}{2M_{\alpha}} \left[2 \mathcal{F}_{JI}^{\alpha}(R) \cdot \nabla_{\alpha} + \tilde{\mathcal{F}}_{JI}^{\alpha}(R) \right] \quad (6)$$

where the sum runs over all nuclear indices α and M_{α} and ∇_{α} denote the corresponding masses and gradients. The latter are usually evaluated in Cartesian coordinates. The con-

tributions \mathcal{F}_{JI} and $\tilde{\mathcal{F}}_{JI}$ are given as

$$\mathcal{F}_{JI}^\alpha(R) = \langle \Phi_J(r; R) | \nabla_\alpha | \Phi_I(r; R) \rangle , \quad (7)$$

$$\tilde{\mathcal{F}}_{JI}^\alpha(R) = \langle \Phi_J(r; R) | \nabla_\alpha^2 | \Phi_I(r; R) \rangle = \nabla_\alpha \mathcal{F}_{JI}^\alpha(R) + \sum_K \mathcal{F}_{JK}^\alpha(R) \mathcal{F}_{KI}^\alpha(R) . \quad (8)$$

The last identity shows that $\mathcal{F}_{JI}^\alpha(R)$ is sufficient to describe the coupling.³ Note, however, that it only holds if the electronic wave functions form a complete basis.

Semiclassical treatments of nuclear motion⁶ commonly neglect $\tilde{\mathcal{F}}_{JI}^\alpha(R)$ and consider only $\mathcal{F}_{JI}^\alpha(R)$, which is called derivative coupling or NAC. Although it has been argued that the other term, $\tilde{\mathcal{F}}_{JI}^\alpha(R)$, in general cannot be neglected,^{7,8} it has also been shown how to account for it in the simulation of non-adiabatic dynamics.⁹ The impact of $\tilde{\mathcal{F}}_{JI}^\alpha(R)$ on the final results appears to be limited.

The elements of the NAC vector can be evaluated by noticing that for an exact solution of the electronic Schrödinger equation, the nuclear gradient of state I (\mathbf{G}_I) satisfies the Hellman-Feynman theorem,

$$G_I^\alpha \equiv \nabla_\alpha \langle \Phi_I | \hat{H}^{el} | \Phi_I \rangle = \langle \Phi_I | (\nabla_\alpha \hat{H}^{el}) | \Phi_I \rangle . \quad (9)$$

By generalization to off-diagonal matrix elements, i.e., interstate couplings, one obtains for $\mathcal{F}_{JI}^\alpha(R)$

$$0 = \nabla_\alpha \langle \Phi_I | \hat{H}^{el} | \Phi_J \rangle = (E_I - E_J) \langle \Phi_I | \nabla_\alpha | \Phi_J \rangle + \langle \Phi_I | (\nabla_\alpha \hat{H}^{el}) | \Phi_J \rangle . \quad (10)$$

From Eq. (10) it follows that the derivative coupling can be evaluated as

$$\mathcal{F}_{IJ}^\alpha(R) = \frac{\langle \Phi_I | (\nabla_\alpha \hat{H}^{el}) | \Phi_J \rangle}{E_J - E_I} \quad (11)$$

where $h_{IJ}^\alpha \equiv \langle \Phi_I | (\nabla_\alpha \hat{H}^{el}) | \Phi_J \rangle$ can be viewed as an interstate generalization of the nuclear gradient that is called the NAC force.^{6,21} Eq. (11) illustrates that the derivative coupling

becomes large when two potential energy surfaces are nearly degenerate. Since $\mathcal{F}_{JI}^\alpha(R)$ enters the Schrödinger equation for the nuclei, Eq. (5), through the scalar product with the nuclear velocity in Eq. (6), non-adiabatic transitions are also more likely when the nuclei move fast. Conversely, the adiabatic approximation is recovered when the nuclei are moving infinitesimally slow. We note that the sign of the vectors h_{IJ} and \mathcal{F}_{IJ} is arbitrary: A change of phase in either Φ_I or Φ_J induces a sign change in h_{IJ} and \mathcal{F}_{IJ} but the resulting wave function is still a solution to Eq. (3). Also, the elements of h_{IJ} and \mathcal{F}_{IJ} sum up to zero because of translational invariance.^{64,65}

2.2 Non-adiabatic coupling between resonances based on complex absorbing potentials

The practitioners of bound-state quantum chemistry need not be concerned that the $|\Phi_I(r; R)\rangle$ in Eq. (2) only form a complete basis if continuum states are included as they work with a basis-set representation of finite size. However, this needs to be reconsidered when dealing with NACs where one or both of the coupled states is an electronic resonance because these states are embedded in the continuum.²⁹⁻³¹

Although it is possible to extend the BO ansatz to Hilbert spaces of infinite dimensions,³ we will follow the conventional approach here and work with a finite set of electronic functions. We accomplish this in the framework of non-Hermitian quantum chemistry where electronic resonances are described as discrete states separated from continuum. In contrast, in Hermitian quantum chemistry, resonances are not discrete states but correspond to an increased density of continuum states.

Our computational treatment of NAC employs the Siegert representation of electronic resonances.³⁵ This means that we consider eigenstates of the electronic Hamiltonian that diverge exponentially in space and have complex energy

$$E_{\text{res}} = E - i\Gamma/2 . \tag{12}$$

The real part of the energy corresponds to the position of the resonance, whereas the imaginary part is related to the decay width Γ . For bound states, $\Gamma = 0$. The Siegert states can be included in the manifold of electronic wave functions $|\Phi_I(r; R)\rangle$ in Eq. (2) in a straightforward manner. E_{res} from Eq. (12) then depends parametrically on the nuclear coordinates and the resonance width Γ is a local quantity.

Alternatively, Eq. (12) can be obtained following the theory by Feshbach and Fano.^{36–38} Importantly, Γ is a non-local quantity in this framework. We discuss the treatment of non-adiabatic effects based on this latter approach in Sec. 2.3. Also, we note that the coupling between diabatic resonance states and the ensuing nuclear dynamics have been analyzed in Ref. 45.

Siegert states and energies can be computed using different techniques, in particular using complex scaling^{66,67} or, alternatively, complex absorbing potentials (CAPs).^{68,69} Here, we use the CAP method where an imaginary potential $\hat{W}(r)$ is added to the electronic Hamiltonian \hat{H}^{el} according to

$$\hat{H}^{\text{el}}(\eta) = \hat{H}^{\text{el}} - i\eta \hat{W}(r). \quad (13)$$

Different functional form have been suggested for \hat{W} , all of which bring the diverging resonance wave function into an \mathcal{L}^2 -integrable form. Here we use a shifted quadratic potential defined as

$$\hat{W}(r) = \hat{W}_x(x) + \hat{W}_y(y) + \hat{W}_z(z)$$

$$\hat{W}_\alpha(\alpha) = \begin{cases} 0 & \text{if } |\alpha - o_\alpha| \leq r_\alpha^0 \\ (|\alpha - o_\alpha| - r_\alpha^0)^2 & \text{otherwise} \end{cases}, \quad \alpha = (x, y, z) \quad (14)$$

where (r_x^0, r_y^0, r_z^0) and (o_x^0, o_y^0, o_z^0) are the onset and origin in each dimension and η is a strength parameter.

The CAP Hamiltonian $\hat{H}^{\text{el}}(\eta)$ has complex eigenvalues and it can be shown that some of them converge to true Siegert energies defined according to Eq. (12) in the limit $\eta \rightarrow 0^+$.⁶⁹ However, in a finite basis set where $\hat{H}^{\text{el}}(\eta)$ is represented approximately, this limit is not

meaningful. In this work, we follow the most common strategy and determine an optimal CAP strength η_{opt} by minimizing the perturbation of the energy in first order, which yields the criterion $\min|\eta dE/d\eta|$.⁶⁹ The remaining eigenvalues of $\hat{H}(\eta)$, which do not correspond to resonances, are either bound states with real energy or pseudocontinuum states whose complex energy changes much more rapidly with η than that of resonances so that no η_{opt} can be determined.

To derive equations for the nuclear motion, we reconsider Eqs. (1) and (2) and assume that some electronic wave functions $|\Phi_I(r; R)\rangle$ have complex energy. Eqs. (4) and (5) do not formally change, but the potential energy surface $E_J(R)$ is complex-valued if one projects onto a resonance state $\langle\Phi_J(r; R)|$. If $\langle\Phi_J(r; R)|$ is a bound state, $E_J(R)$ is real-valued whereas $\hat{\Lambda}_{JI}$ is complex-valued for all I that correspond to resonance states.

The definitions of the coupling matrix elements, Eqs. (6)–(8), do not change when one or both of the coupled states have complex energy. Also, it is still possible to evaluate the derivative coupling from the NAC force through Eq. (11). This shows that the derivative coupling diverges at exceptional points where the real and imaginary parts of two resonance energies E_I and E_J become identical. An important difference between real-valued and complex-valued NAC is also apparent from Eq. (11): The vectors \mathcal{F}_{IJ} and h_{IJ} are necessarily collinear if E_I and E_J are both real but this is not the case if one or both of them are complex. Rather, the four vectors $\text{Re}(\mathcal{F}_{IJ})$, $\text{Im}(\mathcal{F}_{IJ})$, $\text{Re}(h_{IJ})$, and $\text{Im}(h_{IJ})$ can all point in different directions.

2.3 Non-adiabatic coupling between resonances based on Feshbach’s projection formalism

As an alternative to CAPs, Feshbach’s projection formalism can be used to define resonance states. In the following, we use the ansatz by O’Malley,⁴⁰ later extended by Royal *et al.*,⁴⁷ to obtain further insights into NAC between resonance states and the meaning of complex-valued NAC vectors between Siegert states obtained from CAP calculations.

In the Feshbach formalism,³⁶⁻³⁹ the total wave function $|\Psi(r, R)\rangle$ from Eq. (1) is expressed as

$$|\Psi\rangle = \hat{Q}|\Psi\rangle + \hat{P}|\Psi\rangle = |\Psi_Q\rangle + |\Psi_P\rangle \quad (15)$$

where the projectors \hat{Q} and \hat{P} operate on the electronic part of the total wave function and are defined as

$$\hat{Q} = \sum_I^n |\Phi_I(r; R)\rangle \langle \Phi_I(r; R)| , \quad (16)$$

$$\hat{P} = 1 - \hat{Q} = \int_0^\infty dE |\chi_E\rangle \langle \chi_E| \quad (17)$$

with $|\Phi_I(r; R)\rangle$ as discrete L^2 -normalized electronic resonance states and $|\chi_E\rangle$ as δ -normalized scattering states. Using Eq. (2) one obtains for $|\Psi_Q\rangle$ the explicit form

$$|\Psi_Q(r, R)\rangle = \sum_I |\Phi_I(r; R)\rangle \xi_I(R) . \quad (18)$$

Applying the Hamiltonian to Eq. (15) yields the following coupled equations:

$$\hat{P}(\hat{H} - \mathcal{E}) \hat{P}|\Psi\rangle = -\hat{P}\hat{H}\hat{Q}|\Psi\rangle , \quad (19)$$

$$\hat{Q}(\hat{H} - \mathcal{E}) \hat{Q}|\Psi\rangle = -\hat{Q}\hat{H}\hat{P}|\Psi\rangle . \quad (20)$$

By plugging Eq. (19) into Eq. (20), a projected Schrödinger equation is obtained for the discrete states, which reads

$$\hat{Q}\hat{H}\hat{Q}|\Psi_Q\rangle + \left[\hat{Q}\hat{H}\hat{P}(\mathcal{E} - \hat{P}\hat{H}\hat{P})^{-1} \hat{P}\hat{H}\hat{Q} \right] |\Psi_Q\rangle = \mathcal{E} |\Psi_Q\rangle . \quad (21)$$

Here, the projected Hamiltonian $\hat{Q}\hat{H}\hat{Q}$ is corrected by a complex level-shift operator \mathcal{S}

defined by

$$\begin{aligned}
\mathcal{S} &= \hat{Q}\hat{H}\hat{P}(\mathcal{E} - \hat{P}\hat{H}\hat{P})^{-1}\hat{P}\hat{H}\hat{Q} = \hat{Q}\hat{H}\hat{P}G_P\hat{P}\hat{H}\hat{Q} \\
&= \sum_{IJ}^n |\Phi_I(r; R)\rangle\langle\Phi_I(r; R)| \hat{H}^{el} P G_P P \hat{H}^{el} |\Phi_J(r; R)\rangle\langle\Phi_J(r; R)| \\
&= \sum_{IJ}^n |\Phi_I(r; R)\rangle \mathcal{S}_{IJ} \langle\Phi_J(r; R)|
\end{aligned} \tag{22}$$

with $G_P = \lim_{\epsilon \rightarrow 0} (\mathcal{E} - \hat{P}\hat{H}\hat{P} + i\epsilon)$ as Green's function in the P -space.

By integrating over the electronic coordinates, one obtains from Eq. (21) the following equation for the nuclear wave function^{40,44,47}

$$\left[\hat{T}_n + E_J(R) + \mathcal{S}_{JJ}(R) \right] |\xi_J(R)\rangle + \sum_I \left[\hat{\Lambda}_{JI} + \mathcal{S}_{JI} \right] |\xi_I(R)\rangle = \mathcal{E} |\xi_J(R)\rangle . \tag{23}$$

Eq. (23) governs nuclear motion in the resonance state and is the equivalent of Eq. (5). The first term describes the motion on an isolated resonance PES while the second term is the NAC. Evidently, both terms include energy-dependent and non-local contributions due to \mathcal{S} that are absent in Eq. (5).

It is, however, often possible to invoke a local complex potential approximation, which results in the boomerang model.⁵⁴⁻⁵⁶ This yields for the elements of \mathcal{S}

$$\mathcal{S}_{II} = \Delta_I - i\Gamma_I/2 \quad \text{for } I = J , \tag{24}$$

$$\mathcal{S}_{IJ} = -i\sqrt{\Gamma_I\Gamma_J}/2 \quad \text{for } I \neq J , \tag{25}$$

where Δ_I represents an energy shift, which is set to zero in the coupling term \mathcal{S}_{IJ} . Evidently, the coupling term \mathcal{S}_{IJ} vanishes if one of the coupled states is bound ($\Gamma = 0$). Likewise, the diagonal term \mathcal{S}_{II} vanishes for bound states as well.

Eqs. (23)–(25) provide a basis for the interpretation of NACs obtained from CAP calculations. In the Feshbach formalism, $\hat{\Lambda}_{JI}$ describes the NAC between two discrete states and

the resonance character comes about solely due to \mathcal{S}_{IJ} . This suggests to associate $\text{Im}(\mathcal{F}_{IJ})$ obtained in a CAP calculation with \mathcal{S}_{IJ} and to interpret $\text{Re}(\mathcal{F}_{IJ})$ as an analog of the NAC between bound states. However, this comparison is problematic for at least two reasons: First, \mathcal{S}_{IJ} does not depend on the nuclear coordinates, meaning it should provide the same contribution to all elements of the NAC vector, whereas $\text{Im}(\mathcal{F}_{IJ})$ inherently depends on the nuclei so that all elements of the vector are different. Second, all results obtained in a CAP calculation are subject to an unwanted dependence on the CAP strength η .

We note that recent experiments²⁴ provide a concrete illustration that non-adiabatic transitions between resonances are modulated by specific vibrations, which can only be explained by the dependence of NACs on nuclear coordinates. However, these observations do not rule out that only the real part of the NAC vector depends on the nuclear coordinates and the imaginary part is coordinate independent.

2.4 Evaluation of non-adiabatic couplings within CAP-EOM-CC framework

The computation of NACs between bound states within the EOM-CC framework has been discussed in Refs. 18–22. Notably, the different formulations are not numerically identical. The recent the work of Kjønstad and Koch²² as well as the earlier work by Christiansen¹⁸ employ CC response theory. In Ref. 22, the NAC is obtained from a biorthonormal formulation in which only the right state is differentiated. In contrast, the works by Ichino *et al.*,¹⁹ by Tajti and Szalay,²⁰ and by Faraji *et al.*²¹ use CC gradient theory.

Here, we use the second strategy, more specifically, the summed-state approach introduced by Tajti and Szalay,²⁰ and combine it with analytic-gradient theory for CAP methods.⁶¹ This allows us to compute NACs between CAP-EOM-CCSD states.

In EOM-CC theory,^{70–75} target states $|\Phi_I\rangle, |\Phi_J\rangle, \dots$ are defined by applying configuration

interaction (CI) like linear excitation operators R_I, R_J, \dots to the CC reference state

$$|\Phi_I\rangle = R_I |\Phi_{\text{ref}}\rangle = R_I e^T |0\rangle \quad (26)$$

where $|0\rangle$ is the reference determinant, usually the Hartree-Fock (HF) determinant, and T stands for the coupled-cluster amplitudes that satisfy the CC equations for the reference state $|\Phi_{\text{ref}}\rangle$. The left EOM-CC states $\langle\Phi_I|, \langle\Phi_J|, \dots$ are not the conjugates of the right EOM-CC states but rather chosen as

$$\langle\Phi_I| = \langle 0| L_I^\dagger e^{-T} \quad (27)$$

where L_I is a CI-like excitation operator as well. The EOM-CC energies and eigenvectors are obtained by solving the eigenvalue equations

$$\bar{H} R_I |0\rangle = E_I R_I |0\rangle, \quad (28)$$

$$\langle 0| L_J^\dagger \bar{H} = E_J \langle 0| L_J^\dagger, \quad (29)$$

$$\langle 0| L_J^\dagger R_I |0\rangle = \delta_{IJ}. \quad (30)$$

where $\bar{H} = e^{-T} \hat{H} e^T$ is the similarity-transformed Hamiltonian.

Depending on the choice of R and L , Eq. (26) and Eq. (27) describe excited, electron-attached, or ionized states. The truncation level of T , R , and L defines the EOM-CCSD, EOM-CCSDT, and so forth models. In the context of this work, where we focus on bound and temporary radical anions, we consider the EOM-EA-CCSD method where R and L are electron-attaching operators comprising one-particle ($1p$) and two-particle-one-hole ($2p1h$) excitations.⁷⁵

To evaluate the NAC between two EOM-CCSD states I and J , we consider an artificial summed state $|\Phi_{I+J}\rangle \equiv |\Phi_I\rangle + |\Phi_J\rangle$ and its gradient \mathbf{G}_{I+J} , which is related to the NAC force

\mathbf{h}_{IJ} according to²⁰

$$\begin{aligned} G_{I+J}^\alpha &= \langle \Phi_{I+J} | (\nabla_\alpha \bar{H}) | \Phi_{I+J} \rangle = \langle \Phi_I | (\nabla_\alpha \bar{H}) | \Phi_I \rangle + \langle \Phi_J | (\nabla_\alpha \bar{H}) | \Phi_J \rangle + 2 \langle \Phi_I | (\nabla_\alpha \bar{H}) | \Phi_J \rangle \\ &= G_I^\alpha + G_J^\alpha + 2 \langle \Phi_I | (\nabla_\alpha \bar{H}) | \Phi_J \rangle = G_I^\alpha + G_J^\alpha + 2 h_{IJ}^\alpha . \end{aligned} \quad (31)$$

From Eq. (31) it follows that the NAC force can be evaluated as

$$h_{IJ}^\alpha = 0.5 (G_{I+J}^\alpha - G_I^\alpha - G_J^\alpha) \quad (32)$$

where the summed-state gradient vector is computed in analogy to the proper gradient vectors \mathbf{G}_I and \mathbf{G}_J . The theory of analytic EOM-CC gradients⁷⁶ is based on the general theory of molecular property calculations in CC theory. For an efficient implementation, the gradient is expressed in terms of differentiated matrix elements over atomic-orbital integrals.

A generic expression is

$$G_I^\alpha = \sum_{\mu\nu} \gamma_{\mu\nu} \mathcal{H}_{\mu\nu}^\alpha + \sum_{\mu\nu\rho\sigma} \Gamma_{\mu\nu\rho\sigma} \langle \mu\nu || \rho\sigma \rangle^\alpha + \sum_{\mu\nu} I_{\mu\nu} S_{\mu\nu}^\alpha \quad (33)$$

where γ , Γ , and \mathbf{I} are density matrices, whose exact definitions depend on the EOM-CC model, and \mathcal{H}^α , $\langle \mu\nu || \rho\sigma \rangle^\alpha$, and S^α are derivatives of the one-electron, two-electron, and overlap integrals.

Because \bar{H} is not symmetric,

$$h_{IJ}^\alpha = \langle \Phi_I | (\nabla_\alpha \bar{H}) | \Phi_J \rangle \neq \langle \Phi_J | (\nabla_\alpha \bar{H}) | \Phi_I \rangle = h_{JI}^\alpha \quad (34)$$

similar to other interstate properties in EOM-CC theory.⁷³ Possible solutions are to consider either the geometric^{19,21} or the arithmetic mean,²⁰ here we choose the former approach.

One concern regarding the computation of the derivative coupling \mathcal{F}_{IJ} is that Eq. (11) does not hold for approximate solutions of the Schrödinger equation. Rather, the result of

Eq. (11) corresponds to a modified derivative coupling \mathcal{F}_{IJ}^C where ∇_α does not operate on the HF wave function but only on the CC and EOM-CC amplitudes.^{20,21} Whereas \mathcal{F}_{IJ}^C is translationally invariant, the full expression, which includes the derivative of the HF wave function, violates translational invariance, which is why it is commonly omitted.^{12,21,65} This is also done in the present work where we use Eq. (11) to compute \mathcal{F}_{IJ}^C .

In a computation of NACs between CAP-EOM-CCSD states, the wave function parameters, energy eigenvalues, and gradient vectors become complex.⁵⁹⁻⁶¹ However, Eqs. (26)-(34) do not formally change except that the usual scalar product is replaced by the c-product.^{29,77} We point out that this is only the case if the CAP is included in the Hamiltonian at the HF level. For projected CAP methods,⁷⁸⁻⁸⁰ which offer the advantage of reduced computational cost, a separate gradient theory would need to be worked out. Importantly, all integrals over atomic orbitals and their derivatives with respect to nuclear displacements are real-valued in CAP-EOM-CCSD, while the density matrices in Eq. (33) are complex-valued. Also, the derivative of the one-electron Hamiltonian \mathcal{H}^α contains some extra terms that result from the differentiation of the CAP and the dependence of the CAP origin on the nuclear coordinates.⁶¹

To analyze the dependence of $h_{IJ}^\alpha = \langle \Phi_I | (\nabla_\alpha \bar{H}(\eta)) | \Phi_J \rangle$ on η , the definition of the CAP Hamiltonian from Eq. (13) can be used. This yields

$$h_{IJ}^\alpha(\eta) = \langle \Phi_I | (\nabla_\alpha \bar{H}) | \Phi_J \rangle - i\eta \langle \Phi_I | (\nabla_\alpha \bar{W}) | \Phi_J \rangle, \quad (35)$$

which illustrates that $h_{IJ}^\alpha(\eta)$ depends linearly on η for large η values. We note that this is similar to the energy but different to molecular properties that can be formulated as expectation values. For the latter quantities, there is no term that depends on η explicitly and the overall dependence on η is determined entirely by that of the density matrix.⁸¹ Eq. (35) suggests that $h_{IJ}^\alpha(\eta)$ can be de-perturbed in analogy to the energy⁵⁹ by removing the term that depends on η explicitly.

3 Implementation

All expressions for evaluating the NAC force h_{IJ} and the derivative coupling \mathcal{F}_{IJ} are implemented in the Q-Chem electronic structure program.⁸² Our implementation is able to compute couplings between CAP-EOM-EA-CCSD states, between CAP-EOM-IP-CCSD states, and between CAP-EOM-EE-CCSD states. However, couplings between CAP-EOM-EE-CCSD states and the CAP-CCSD reference state are not implemented. Also, our implementation requires to include all electrons in the correlation treatment because the implementation of analytic CAP-EOM-CCSD gradients⁶¹ on which our work is based has the same restriction.

The following steps are taken to compute h_{IJ} and \mathcal{F}_{IJ} :

1. Solve the CAP-HF and CAP-CCSD equations for the reference state.
2. Solve the right and left CAP-EOM-EA-CCSD equations, Eq. (28) and Eq. (29), for the coupled states I and J .
3. Solve the amplitude response and orbital response equations for states I , J , and $I + J$ and construct the density matrices $\boldsymbol{\gamma}$, $\boldsymbol{\Gamma}$, and \mathbf{I} for each state.
4. Evaluate the gradient vectors \mathbf{G}_I , \mathbf{G}_J , and \mathbf{G}_{I+J} using Eq. (33).
5. Compute NAC forces h_{IJ} using Eq. (32) and derivative couplings \mathcal{F}_{IJ} using Eq. (11).

To verify our implementation, we evaluated the summed-state gradient \mathbf{G}_{I+J} through numerical differentiation. Note that special attention has to be paid to the relative phase of the two coupled states in these calculations.

4 Computational details

As an illustration of complex-valued NACs between CAP-EOM-EA-CCSD states, we consider anionic states of fumaronitrile (trans-CN-CH=CH-CN, point group C_{2h}). We chose

fumaronitrile as an example for the following reasons: First, electron attachment to an out-of-plane π^* molecular orbital (MO) produces a bound anion (2B_g state) with an energy lower than that of the neutral ground state. Second, multiple resonance states with different symmetry exist. Ehara and Sommerfeld reported four anionic resonance states,⁸³ of in-plane (2A_g , 2B_u) and out-of-plane (2A_u , 2B_g) character using the symmetry adapted cluster (SAC)-CI ansatz and a projected CAP.⁷⁹

Here, we consider the bound anion (2B_g) and the resonance states of 2A_g and 2A_u symmetry and compute the NAC between bound and pseudocontinuum states, between bound and resonance states, and between two resonance states. The geometry of neutral fumaronitrile was optimized in the xy -plane using B3LYP^{84,85}/cc-pVTZ⁸⁶ and is provided in the SI. In the following, we refer to the central carbon atoms of fumaronitrile as C1 and C2, while the outer carbon atoms, which belong to the cyano groups, are named C3 and C4. Note that C1 and C2, C3 and C4, as well as the nitrogen and hydrogen atoms are pairwise equivalent due to symmetry.

In the CAP-EOM-EA-CCSD calculations for the anionic states, we added a set of 2s5p2d diffuse shells to the cc-pVTZ basis on all C and N atoms to achieve satisfactory stabilization of the η -trajectories of the resonance states. For those diffuse shells, the exponent ratios are 1.5 for the p functions and 2.0 for the s and d functions. The resulting basis set is identical to the one from Ref. 83. We used a cuboid CAP with onsets $r_x^0 = 25.460$ a.u., $r_y^0 = 7.039$ a.u., $r_z^0 = 5.047$ a.u. in all calculations.

5 Results

5.1 Energies and decay widths

The vertical electron affinity of fumaronitrile was determined as 0.93 eV using EOM-EA-CCSD/cc-pVTZ+2s5p2d, as compared to the SAC-CI value of 1.01 eV⁸³ and the experimental value for the adiabatic electron affinity of 1.21 eV.⁸⁷

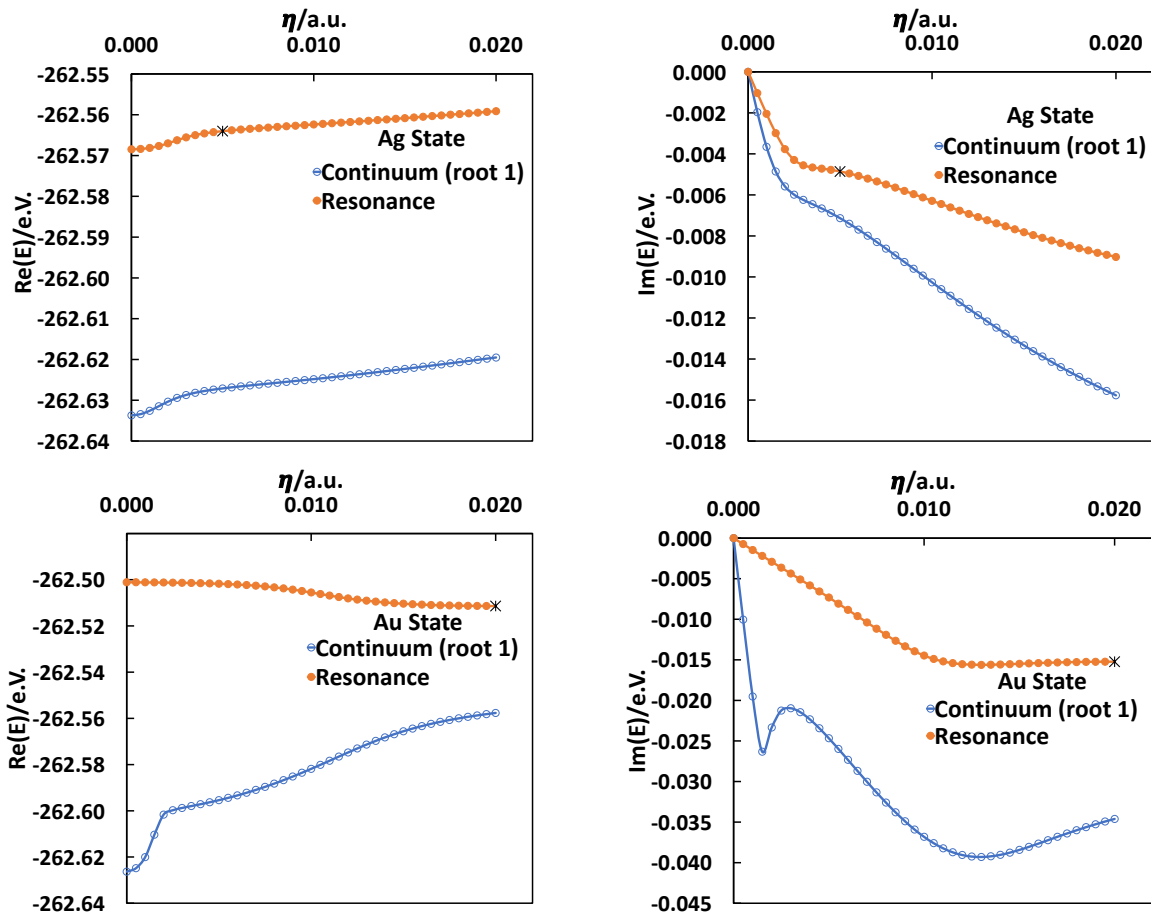


Figure 1: Real (left) and imaginary (right) energies of resonance and pseudocontinuum states of 2A_g (upper panels) and 2A_u (lower panels) symmetry as a function of CAP strength η computed with CAP-EOM-EA-CCSD/cc-pVTZ+2s5p2d at the equilibrium structure of neutral fumaronitrile. Optimal CAP strengths η_{opt} are indicated by black stars.

To identify the resonance states, we analyzed the behavior of the ten lowest CAP-EOM-EA-CCSD states of A_g and A_u symmetry as a function CAP strength η . Figure 1 shows the real and imaginary parts of the energy of the lowest-lying resonance and pseudocontinuum states of both symmetries. In both cases, the resonance state is energetically above the lowest pseudocontinuum state. Figure 1 also illustrates that the stabilization of the A_u resonance is somewhat better than that of the A_g resonance. From these η -trajectories, we determined the η_{opt} values for the 2A_g and 2A_u resonances as 0.005 a.u. and 0.020 a.u., respectively, by means of the criterion $\min|\eta dE/d\eta|$ (see Sec. 2.2).

In addition, we computed the positions and widths of these two resonance states with

projected CAP-EOM-EA-CCSD.⁸⁰ In these calculations, the CAP was constructed in a basis of 10 EOM-EA-CCSD states; the optimal CAP strengths are 0.006 a.u. and 0.021 a.u., respectively, for the 2A_g and 2A_u resonances. For both approaches, projected and full CAP-EOM-EA-CCSD, we also computed the first-order correction and analyzed the corresponding trajectories.^{59,69}

All computed resonance positions and widths are given in Table 1. Full and projected CAP-EOM-EA-CCSD agree within 0.03 eV for the positions and widths of both states; only for the first-order corrected resonance position of the 2A_u state, the difference is 0.1 eV. The correction amounts to at most 0.06 eV. In view of this good agreement among different CAP-EOM-EA-CCSD variants, the substantial deviations from CAP-SAC-CI⁸³ that we observe for the 2A_u resonance are somewhat surprising. For this state, the resonance position computed with CAP-EOM-EA-CCSD is 0.5 eV lower than the CAP-SAC-CI value, whereas the resonance width is about twice as large, i.e., 0.8 eV as compared to 0.4 eV. In contrast, we observe good agreement with CAP-SAC-CI for the 2A_g resonance; the position and width differ by no more than 0.15 eV.

We also computed CAP-EOM-EA-CCSD Dyson orbitals⁸¹ for the bound and temporary anion states of fumaronitrile. The real parts of these orbitals are shown in Figure 2. It is evident that the b_g and a_u orbitals have out-of-plane character while the a_g orbital has in-plane character.

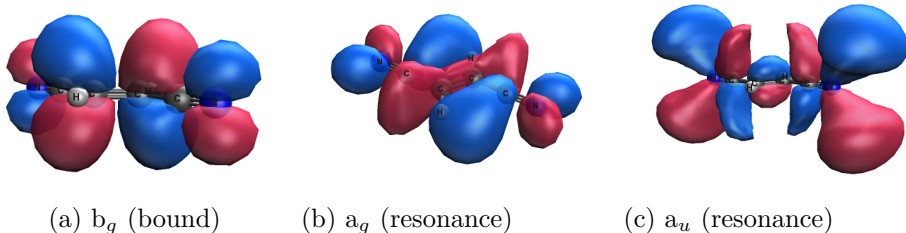


Figure 2: Real parts of Dyson orbitals for electron attachment to fumaronitrile computed with CAP-EOM-EA-CCSD/cc-pVTZ+2s5p2d at the respective η_{opt} and plotted at an isovalue of 0.02.

Table 1: Resonance positions E and widths Γ of fumaronitrile in eV computed with full and projected CAP-EOM-EA-CCSD and projected CAP-SAC-CI. Values are given with and without the first-order correction.

State	full CAP-EOM-EA-CCSD ^a		proj. CAP-EOM-EA-CCSD ^a		proj. CAP-SAC-CI ^b	Expt. ^c
	uncorr.	corr.	uncorr.	corr.		
Resonance positions						
² A _g	2.27	2.21	2.28	2.24	2.35	1.8
² A _u	3.70	3.74	3.67	3.64	4.11	3.5
Resonance widths						
² A _g	0.26	0.31	0.27	0.33	0.39	–
² A _u	0.80	0.82	0.78	0.84	0.37	–

^a This work.

^b From Ref. 83, computed with an approximate symmetrized SAC-CI matrix and a smooth Voronoi CAP.

^c From Ref. 88, determined using electron transmission spectroscopy.

5.2 Non-adiabatic coupling between bound and pseudocontinuum states

Fig. 3 shows the NAC force h and the derivative coupling \mathcal{F} between the lowest pseudocontinuum state of A_g symmetry and the bound ²B_g state of the fumaronitrile anion. Since the sign is arbitrary, we report the absolute values of all elements. We point out that the physical meaning of pseudocontinuum states in CAP theories is limited; the main purpose of Fig. 3 is to enable a discussion of differences between pseudocontinuum states and resonances, which we do in the following sections. In addition, the analysis of coupling vectors involving pseudocontinuum states is helpful for the verification of our implementation. For example, the NAC force vector always needs to reflect spatial symmetry and the sum of all elements needs to vanish for couplings between bound, resonance, and pseudocontinuum states alike.

The two states shown in Fig. 3 are coupled by vibrations of b_g symmetry, which correspond to out-of-plane motions in z direction. Panels *a* and *b* of Fig. 3 illustrate the dependence of the four symmetry-unique elements of h on the CAP strength η , while panels *c* and *d* show the same for the norms of h and \mathcal{F} , respectively. It is apparent that there is no stabilization with respect to η in the imaginary part of either h or \mathcal{F} , which reflects the behavior of the energy of pseudocontinuum states. The asymptotically linear dependence on

η according to Eq. (35) is clearly visible. Somewhat surprisingly, the real part of h does not vary much in the range $\eta = 0.005 - 0.020$ a.u.; only at larger CAP strengths the dependence is more pronounced. Notably, the four elements of h are all of the same order of magnitude, while their dependence on η differs a little.

5.3 Non-adiabatic coupling between bound and resonance states

The NAC force and the derivative coupling between the bound 2B_g state and the 2A_g resonance are shown in Fig. 4. As the irreducible representations are the same as for the pair of states displayed in Fig. 3, the same four symmetry-unique elements of h and \mathcal{F} are non-zero. However, whereas all four elements are of similar magnitude for the coupling to the pseudocontinuum state in Fig. 3, the coupling to the resonance state is dominated by one single element, the out-of-plane motion of the hydrogen atoms. This element of $\text{Re}(h)$ is about 10 times larger than the other three elements of $\text{Re}(h)$ and all four elements of $\text{Im}(h)$. Although the linear dependence on η is visible for large η values, all elements of h vary less with η above $\eta_{\text{opt}} = 0.005$ a.u. than in Fig. 3, especially as concerns the imaginary part. This reflects the behavior of the energy and illustrates that the resonance is stabilized.

It is thus meaningful to evaluate the NAC force at one particular CAP strength as done in panels *a* and *b* of Fig. 4. This graphics illustrates that $\text{Re}(h)$ and $\text{Im}(h)$ point in different directions. More specifically, the angle between these two vectors is 97° . $\text{Re}(h)$ and $\text{Re}(\mathcal{F})$ are nearly collinear, whereas $\text{Im}(h)$ and $\text{Im}(\mathcal{F})$ span an angle of ca. 9° . Although it is difficult to assign physical meaning to these angles, we repeat that h and \mathcal{F} are necessarily collinear in Hermitian quantum chemistry, while this is not the case in non-Hermitian quantum chemistry by virtue of Eq. (11).

The norms of h and \mathcal{F} are displayed in panels *e* and *f* of Fig. 4. Notably, the differences between the pseudocontinuum state and the resonance are less visible here than in the individual elements of h . It is also worth noting that the evaluation of h and \mathcal{F} at $\eta = 0$, i.e., with bound-state EOM-CCSD, gives different results: Although the norms are similar,

the ratio between the elements is markedly different at η_{opt} .

As a second example, shown in Figs. 5 and 6, we investigated the NAC between the bound 2B_g state and the 2A_u resonance. These two states are coupled by vibrations of b_u symmetry, which correspond to motions in the xy plane. There are eight symmetry-unique elements of h , whose dependence on η is displayed in Fig. 5. Similar to Fig. 4, all elements of $\text{Re}(h)$ and $\text{Im}(h)$ do not change much with η above the optimal value, which is 0.020 a.u. for the 2A_u resonance. The two elements of h that correspond to the motion of the hydrogen atoms are almost zero, whereas the atoms of the cyano groups have the largest elements in h . Similar to the previous example, $\text{Re}(h)$ and $\text{Im}(h)$ point in different directions but here the angle between them amounts to ca. 171° . $\text{Re}(h)$ and $\text{Re}(\mathcal{F})$ are again almost collinear and the angle between $\text{Im}(h)$ and $\text{Im}(\mathcal{F})$ is ca. 2° .

An important difference between the two resonance states is that the excitation from the bound 2B_g state to the 2A_u resonance is bright, whereas the excitation to the 2A_g resonance is dark owing to spatial symmetry. We would thus expect that the NAC between the 2B_g and 2A_u states could be probed in a photodetachment experiment on the anion of fumaronitrile if direct and indirect detachment can be distinguished.

For this reason, we investigated the dependence of h and \mathcal{F} on the CN bond distance for the coupling between the 2B_g and 2A_u states. Fig. 6 demonstrates that h and \mathcal{F} are very sensitive to the molecular structure as already a small change of 0.02 Å in the CN distance changes the norms of $\text{Re}(h)$ and $\text{Im}(h)$ by more than 10%. Interestingly, the norm of $\text{Re}(h)$ grows when the CN bond is stretched while the norm of $\text{Im}(h)$ shrinks. We note that the width of the 2A_u state also changes significantly from 0.96 eV over 0.80 eV to 0.63 eV when stretching the bond. However, the energy gap between the two states only changes from 4.60 eV to 4.63 eV as both anionic states are stabilized with respect to the neutral ground state when the CN bond is stretched. This can be explained by the shape of the Dyson orbitals shown in Fig. 2, both of which have nodal planes across the CN bond.

5.4 Non-adiabatic coupling between two resonance states

As a final example, we studied the coupling between the 2A_g and the 2A_u resonance, which is mediated by vibrations of a_u symmetry. This means that the only non-zero elements of h and \mathcal{F} are in z -direction. However, as illustrated by Fig. 7, there is no stabilization of $\text{Re}(h)$ or $\text{Im}(h)$ with respect to η because the two resonances have different optimal CAP strengths. Fig. 7 shows that the NAC force has significantly different character at the two respective η_{opt} values of 0.005 a.u. and 0.02 a.u. At the lower value, the vector is dominated by the elements corresponding to movements of the carbon atoms, but their magnitude is much smaller at the higher value. We note that the lack of stability with respect to η was also observed for transition dipole moments between two resonances computed with CAP-EOM-CCSD⁸¹ and can be considered a fundamental weakness of CAP methods. Also noteworthy is that $\text{Re}(h)$ and $\text{Im}(h)$ are of similar magnitude, which is different from the coupling between a resonance and a bound state where the real part is dominant (see Sec. 5.3).

6 Conclusions

We presented the theory and implementation of NAC vectors within the CAP-EOM-EA-CCSD framework, which is relevant for the study of non-adiabatic effects involving molecular temporary anions. Our approach is based on the Siegert representation, where electronic resonances are adiabatic states with complex energy and the resonance width is a local quantity. We also considered the connection of our approach to the treatment of NACs based on the Feshbach representation of electronic resonances.

The use of analytic gradient theory for CAP methods enables a treatment of polyatomic molecules that takes account of the full dimensionality of their PESs. We demonstrated this in a pilot application to anionic states of fumaronitrile, where we investigated the NACs between bound, resonance, and pseudocontinuum states. Our approach is most useful for

evaluating couplings between a resonance and a bound state, where the results depend only weakly on the CAP strength. In contrast, couplings between two resonances depend more strongly on the CAP strength, which arises from a fundamental feature of CAP methods, namely, that optimal CAP parameters are specific to a particular resonance state.

We see our work as a step towards the modeling of non-adiabatic effects involving metastable states in polyatomic molecules. Given the shortcomings of the CAP approach, it appears worthwhile to extend other approaches for electronic resonances to NACs. At the same time, we are convinced that our method is already useful in its present form as there are numerous other bound molecular anions besides fumaronitrile that have metastable excited states. NACs between them should leave fingerprints in spectroscopic experiments and we believe that NAC vectors computed with our method could help model them.

Acknowledgements

This work was supported in Los Angeles by the U.S. National Science Foundation (CHE-2154482 to A.I.K.) and in Leuven by the European Research Council (ERC) under the European Union’s Horizon 2020 research and innovation program (Grant No. 851766 to T.C.J.) and the KU Leuven internal funds (Grant C14/22/083).

Conflicts of interest

The authors declare the following competing financial interest(s): A.I.K. is the president and a part-owner of Q-Chem, Inc.

Data availability

The data that support the findings of this study are available within the article and the associated SI.

References

- (1) Born, M.; Oppenheimer, R. Zur Quantentheorie der Molekeln. *Ann. Phys.* **1927**, *389*, 457–484.
- (2) Köppel, H.; Domcke, W.; Cederbaum, L. S. Multimode Molecular Dynamics Beyond the Born-Oppenheimer Approximation. *Adv. Chem. Phys.* **2007**, *57*, 59–246.
- (3) Baer, M. Introduction to the theory of electronic non-adiabatic coupling terms in molecular systems. *Phys. Rep.* **2002**, *2002*, 75–142.
- (4) Yarkony, D. R. Nonadiabatic Quantum Chemistry—Past, Present, and Future. *Chem. Rev.* **2012**, *112*, 481–498.
- (5) Curchod, B. F. E.; Martínez, T. J. Ab Initio Nonadiabatic Quantum Molecular Dynamics. *Chem. Rev.* **2018**, *118*, 3305–3336.
- (6) Matsika, S. Electronic Structure Methods for the Description of Nonadiabatic Effects and Conical Intersections. *Chem. Rev.* **2021**, *121*, 9407–9449.
- (7) Reimers, J. R.; McKemmish, L. K.; McKenzie, R. H.; Hush, N. S. Non-adiabatic effects in thermochemistry, spectroscopy and kinetics: the general importance of all three Born-Oppenheimer breakdown corrections. *Phys. Chem. Chem. Phys.* **2015**, *17*, 24641–24665.
- (8) Meek, G. A.; Levine, B. G. Wave function continuity and the diagonal Born-Oppenheimer correction at conical intersections. *J. Chem. Phys.* **2016**, *144*, 184109.
- (9) Meek, G. A.; Levine, B. G. The best of both Reprs—Diabatized Gaussians on adiabatic surfaces. *J. Chem. Phys.* **2016**, *145*, 184103.
- (10) Tapavicza, E.; Bellchambers, G. D.; Vincenta, J. C.; Furche, F. Ab initio non-adiabatic molecular dynamics. *Phys. Chem. Chem. Phys.* **2013**, *15*, 18336–18348.

- (11) Ou, Q.; Fatehi, S.; Alguire, E.; Shao, Y.; Subotnik, J. E. Derivative couplings between TDDFT excited states obtained by direct differentiation in the Tamm-Dancoff approximation. *J. Chem. Phys.* **2014**, *141*, 024114.
- (12) Zhang, X.; Herbert, J. M. Analytic derivative couplings for spin-flip configuration interaction singles and spin-flip time-dependent density functional theory. *J. Chem. Phys.* **2014**, *141*, 064104.
- (13) Zhang, X.; Herbert, J. M. Analytic derivative couplings in time-dependent density functional theory: Quadratic response theory versus pseudo-wavefunction approach. *J. Chem. Phys.* **2015**, *142*, 064109.
- (14) Lengsfeld, B. H.; Saxe, P.; Yarkony, D. R. On the evaluation of nonadiabatic coupling matrix elements using SA-MCSCF/CI wave functions and analytic gradient methods. I. *J. Chem. Phys.* **1984**, *81*, 4549–4553.
- (15) Galván, I. F.; Delcey, M. G.; Pedersen, T. B.; Aquilante, F.; Lindh, R. Analytical State-Average Complete-Active-Space Self-Consistent Field Nonadiabatic Coupling Vectors: Implementation with Density-Fitted Two-Electron Integrals and Application to Conical Intersections. *J. Chem. Theory Comput.* **2016**, *12*, 3636–3653.
- (16) Saxe, P.; Lengsfeld, B. H.; Yarkony, D. R. On the evaluation of non-adiabatic coupling matrix elements for large scale CI wavefunctions. *Chem. Phys. Lett.* **1985**, *113*, 159–164.
- (17) Lischka, H.; Dallos, M.; Szalay, P. G.; Yarkony, D. R.; Shepard, R. Analytic evaluation of nonadiabatic coupling terms at the MR-CI level. I. Formalism. *J. Chem. Phys.* **2004**, *120*, 7322–7329.
- (18) Christiansen, O. First-order nonadiabatic coupling matrix elements using coupled cluster methods. I. Theory. *J. Chem. Phys.* **1999**, *110*, 711–723.

- (19) Ichino, T.; Gauss, J.; Stanton, J. F. Quasidiabatic states described by coupled-cluster theory. *J. Chem. Phys.* **2009**, *130*, 174105.
- (20) Tajti, A.; Szalay, P. G. Analytic evaluation of the nonadiabatic coupling vector between excited states using equation-of-motion coupled-cluster theory. *J. Chem. Phys.* **2009**, *131*, 124104.
- (21) Faraji, S.; Matsika, S.; Krylov, A. I. Calculations of non-adiabatic couplings within equation-of-motion coupled-cluster framework: Theory, implementation, and validation against multi-reference methods. *J. Chem. Phys.* **2018**, *148*, 044103.
- (22) Kjørstad, E. F.; Koch, H. Communication: Non-adiabatic derivative coupling elements for the coupled cluster singles and doubles model. *J. Chem. Phys.* **2023**, *158*, 161106.
- (23) Mukherjee, M.; Ragesh Kumar, T. P.; Ranković, M.; Nag, P.; Fedor, J.; Krylov, A. I. Spectroscopic signatures of states in the continuum characterized by a joint experimental and theoretical study of pyrrole. *J. Chem. Phys.* **2022**, *157*, 204305.
- (24) Kumar, T. P. R.; Nag, P.; Ranković, M.; Luxford, T. F. M.; Kocíšek, J.; Masín, Z.; Fedor, J. Distant Symmetry Control in Electron-Induced Bond Cleavage. *J. Phys. Chem. Lett.* **2022**, *13*, 11136–11142.
- (25) West, C. W.; Bull, J. N.; Antonkov, E.; Verlet, J. R. R. Anion Resonances of *para*-Benzoquinone Probed by Frequency-Resolved Photoelectron Imaging. *J. Phys. Chem. A* **2014**, *118*, 11346–11354.
- (26) Mensa-Bonsu, G.; Wilson, M. R.; Tozer, D. J.; Verlet, J. R. R. Photoelectron spectroscopy of *para*-benzoquinone cluster anions. *J. Chem. Phys.* **2019**, *151*, 204302.
- (27) Nag, P.; Tarana, M.; Fedor, J. Effects of π^* - σ^* coupling on dissociative-electron-attachment angular distributions in vinyl, allyl, and benzyl chloride and in chlorobenzene. *Phys. Rev. A* **2021**, *103*, 032830.

- (28) Kumar, S.; Izadi, F.; Ončák, M.; Limão-Vieira, P.; Denifl, S. Hexachlorobenzene-negative ion formation in electron attachment experiments. *Phys. Chem. Chem. Phys.* **2022**, *24*, 13335–13342.
- (29) Moiseyev, N. *Non-Hermitian Quantum Mechanics*; Cambridge University Press, 2011.
- (30) Jagau, T.-C.; Bravaya, K. B.; Krylov, A. I. Extending Quantum Chemistry of Bound States to Electronic Resonances. *Annu. Rev. Phys. Chem.* **2017**, *68*, 525–553.
- (31) Jagau, T.-C. Theory of electronic resonances: fundamental aspects and recent advances. *Chem. Commun.* **2022**, *58*, 5205–5224.
- (32) Bardsley, J. N.; Mandl, F. Resonant scattering of electrons by molecules. *Rep. Prog. Phys.* **1968**, *31*, 471–531.
- (33) Taylor, J. R. *Scattering Theory: The Quantum Theory on Nonrelativistic Collisions*; Wiley, 1971.
- (34) Gamov, G. Zur Quantentheorie des Atomkernes. *Z. Phys.* **1928**, *51*, 204–212.
- (35) Siegert, A. J. F. On the Derivation of the Dispersion Formula for Nuclear Reactions. *Phys. Rev.* **1939**, *56*, 750–752.
- (36) Feshbach, H. Unified theory of nuclear reactions. *Ann. Phys. (N. Y.)* **1958**, *5*, 357–390.
- (37) Fano, U. Effects of Configuration Interaction on Intensities and Phase Shifts. *Phys. Rev.* **1961**, *124*, 1866–1878.
- (38) Feshbach, H. A unified theory of nuclear reactions. II. *Ann. Phys. (N. Y.)* **1962**, *19*, 287–313.
- (39) Domcke, W. Theory of resonance and threshold effects in electron-molecule collisions: The projection-operator approach. *Physics Reports* **1991**, *208*, 97–188.
- (40) O'Malley, T. F. Theory of dissociative attachment. *Phys. Rev.* **1966**, *150*, 14–29.

- (41) Domcke, W.; Cederbaum, L. S. Theory of the vibrational structure of resonances in electron-molecule scattering. *Phys. Rev. A* **1977**, *16*, 1465–1482.
- (42) Hazi, A. U. Effects of resonance-resonance coupling on dissociative electron attachment. *J. Phys. B At. Mol. Phys.* **1983**, *16*, L29–L34.
- (43) Bieniek, R. J. Complex Potential and electron spectrum in atomic collisions involving fast electronic transitions: Penning and associative ionization. *Phys. Rev. A* **1983**, *18*, 392–413.
- (44) Domcke, W.; Berman, M.; Estrada, H.; Mündel, C.; Cederbaum, L. S. Aspects of Nuclear Dynamics In Short-Lived Negative Ion States. *J. Phys. Chem.* **1984**, *88*, 4862–4867.
- (45) Estrada, H.; Cederbaum, L. S.; Domcke, W. Vibronic coupling of short-lived electronic states. *J. Chem. Phys.* **1986**, *84*, 152–169.
- (46) Cederbaum, L. S.; Friedman, R. S.; Ryaboy, V. M.; Moiseyev, N. Conical Intersections and Bound Molecular States Embedded in the Continuum. *Phys. Rev. Lett.* **2003**, *90*, 013001.
- (47) Royal, J.; Larson, Å.; Orel, A. E. Effect of couplings in the resonance continuum. *J. Phys. B At. Mol. Opt. Phys.* **2004**, *37*, 3075–3083.
- (48) Feuerbacher, S.; Sommerfeld, T.; Cederbaum, L. S. Intersections of potential energy surfaces of short-lived states: The complex analogue of conical intersections. *J. Chem. Phys.* **2004**, *120*, 3201–3214.
- (49) Haxton, D. J.; McCurdy, C. W.; Rescigno, T. N. Dissociative electron attachment to the H₂O molecule. I. Complex-valued potential-energy surfaces for the ²B₁, ²A₁, and ²B₂ metastable states of the water anion. *Phys. Rev. A* **2007**, *75*, 012710.

- (50) Haxton, D. J.; McCurdy, C. W.; Rescigno, T. N. Dissociative electron attachment to the H₂O molecule. II. Nuclear dynamics on coupled electronic surfaces within the local complex potential model. *Phys. Rev. A* **2007**, *75*, 012711.
- (51) Benda, Z.; Jagau, T.-C. Locating Exceptional Points on Multidimensional Complex-Valued Potential Energy Surfaces. *J. Phys. Chem. Lett.* **2018**, *9*, 6978–6984.
- (52) Gyamfi, J. A.; Jagau, T.-C. Ab Initio Molecular Dynamics of Temporary Anions Using Complex Absorbing Potentials. *J. Phys. Chem. Lett.* **2022**, *13*, 8477–8483.
- (53) Cederbaum, L. S.; Domcke, W. Local against non-local complex potential in resonant electron-molecule scattering. *J. Phys. B At. Mol. Phys.* **1981**, *14*, 4665–4689.
- (54) Herzenberg, A. Oscillatory energy dependence of resonant electron-molecule scattering. *J. Phys. B At. Mol. Phys.* **1968**, *1*, 548.
- (55) Birtwistle, D. T.; Herzenberg, A. Vibrational excitation of N₂ by resonance scattering of electrons. *J. Phys. B At. Mol. Phys.* **1971**, *4*, 53–70.
- (56) Dubé, L.; Herzenberg, A. Resonant electron-molecule scattering: The impulse approximation in N₂O. *Phys. Rev. A* **1975**, *11*, 1314–1325.
- (57) Dubé, L.; Herzenberg, A. Absolute cross sections from the "boomerang model" for resonant electron-molecule scattering. *Phys. Rev. A* **1979**, *20*, 194–213.
- (58) Ghosh, A.; Vaval, N.; Pal, S. Equation-of-motion coupled-cluster method for the study of shape resonance. *J. Chem. Phys.* **2012**, *136*, 234110.
- (59) Jagau, T.-C.; Zuev, D.; Bravaya, K. B.; Epifanovsky, E.; Krylov, A. I. A Fresh Look at Resonances and Complex Absorbing Potentials: Density Matrix-Based Approach. *J. Phys. Chem. Lett.* **2014**, *5*, 310–315.
- (60) Zuev, D.; Jagau, T.-C.; Bravaya, K. B.; Epifanovsky, E.; Shao, Y.; Sundstrom, E.; Head-Gordon, M.; Krylov, A. I. Complex absorbing potentials within EOM-CC family

- of methods: Theory, implementation, and benchmarks. *J. Chem. Phys.* **2014**, *141*, 024102.
- (61) Benda, Z.; Jagau, T.-C. Communication: Analytic gradients for the complex absorbing potential equation-of-motion coupled-cluster method. *J. Chem. Phys.* **2017**, *146*, 031101.
- (62) Benda, Z.; Rickmeyer, K.; Jagau, T.-C. Structure Optimization of Temporary Anions. *J. Chem. Theory Comput.* **2018**, *14*, 3468–3478.
- (63) Benda, Z.; Jagau, T.-C. Understanding Processes Following Resonant Electron Attachment: Minimum-Energy Crossing Points between Anionic and Neutral Potential Energy Surfaces. *J. Chem. Theory Comput.* **2018**, *14*, 4216–4223.
- (64) Tommasini, M.; Chernyak, V.; Mukamel, S. Electronic Density-Matrix Algorithm for Nonadiabatic Couplings in Molecular Dynamics Simulations. *Int. J. Quantum Chem.* **2001**, *85*, 225–238.
- (65) Fatehi, S.; Alguire, E.; Shao, Y.; Subotnik, J. E. Analytic derivative couplings between configuration-interaction singles states with built-in electron-translation factors for translational invariance. *J. Chem. Phys.* **2011**, *135*, 234105.
- (66) Aguilar, J.; Combes, J. M. A class of analytic perturbations for one-body Schrödinger Hamiltonians. *Commun. Math. Phys.* **1971**, *22*, 269–279.
- (67) Balslev, E.; Combes, J. M. Spectral properties of many-body Schrödinger operators with dilatation-analytic interactions. *Commun. Math. Phys.* **1971**, *22*, 280–294.
- (68) Jolicard, G.; Austin, E. J. Optical potential stabilisation method for predicting resonance levels. *Chem. Phys. Lett.* **1985**, *121*, 106–110.
- (69) Riss, U. V.; Meyer, H. D. Calculation of resonance energies and widths using the

- complex absorbing potential method. *J. Phys. B At. Mol. Opt. Phys.* **1993**, *26*, 4503–4535.
- (70) Krylov, A. I. Equation-of-Motion Coupled-Cluster Methods for Open-Shell and Electronically Excited Species: The Hitchhiker’s Guide to Fock Space. *Annu. Rev. Phys. Chem.* **2008**, *59*, 433–462.
- (71) Bartlett, R. J. Coupled-cluster theory and its equation-of-motion extensions. *WIREs Comput. Mol. Sci.* **2012**, *2*, 126–138.
- (72) Sekino, H.; Bartlett, R. J. A linear response, coupled-cluster theory for excitation energy. *Int. J. Quantum Chem.* **1984**, *26*, 255–265.
- (73) Stanton, J. F.; Bartlett, R. J. The equation of motion coupled-cluster method. A systematic biorthogonal approach to molecular excitation energies, transition probabilities, and excited state properties. *J. Chem. Phys.* **1993**, *98*, 7029–7039.
- (74) Stanton, J. F.; Gauss, J. Analytic energy derivatives for ionized states described by the equation-of-motion coupled cluster method. *J. Chem. Phys.* **1994**, *101*, 8938–8944.
- (75) Nooijen, M.; Bartlett, R. J. Description of core-excitation spectra by the open-shell electron-attachment equation-of-motion coupled cluster method. *J. Chem. Phys.* **1995**, *102*, 6735–6756.
- (76) Stanton, J. F. Many-body methods for excited state potential energy surfaces. I. General theory of energy gradients for the equation-of-motion coupled-cluster method. *J. Chem. Phys.* **1993**, *99*, 8840–8847.
- (77) Moiseyev, N.; Certain, P.; Weinhold, F. Resonance properties of complex-rotated Hamiltonians. *Mol. Phys.* **1978**, *36*, 1613–1630.
- (78) Sommerfeld, T.; Santra, R. Efficient method to perform CAP/CI calculations for temporary anions. *Int. J. Quantum Chem.* **2001**, *82*, 218–226.

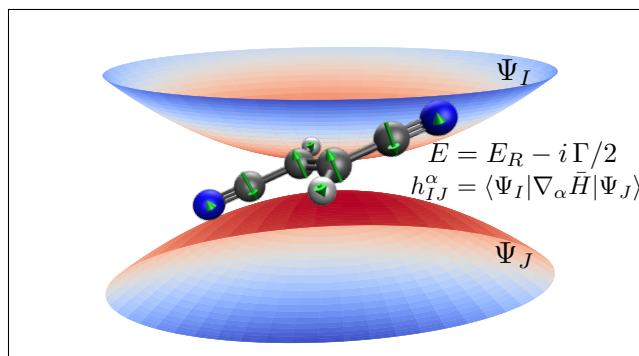
- (79) Ehara, M.; Sommerfeld, T. CAP/SAC-CI method for calculating resonance states of metastable anions. *Chem. Phys. Lett.* **2012**, *537*, 107–112.
- (80) Gayvert, J. R.; Bravaya, K. B. Projected CAP-EOM-CCSD method for electronic resonances. *J. Chem. Phys.* **2022**, *156*, 094108.
- (81) Jagau, T.-C.; Krylov, A. I. Characterizing metastable states beyond energies and lifetimes: Dyson orbitals and transition dipole moments. *J. Chem. Phys.* **2016**, *144*, 054113.
- (82) Epifanovsky, E.; Gilbert, A. T. B.; Feng, X.; Lee, J.; Mao, Y.; Mardirossian, N.; Pokhilko, P.; White, A. F.; Coons, M. P.; Dempwolff, A. L.; Gan, Z.; Hait, D.; Horn, P. R.; Jacobson, L. D.; Kaliman, I.; Kussmann, J.; Lange, A. W.; Lao, K. U.; Levine, D. S.; Liu, J.; McKenzie, S. C.; Morrison, A. F.; Nanda, K. D.; Plasser, F.; Rehn, D. R.; Vidal, M. L.; You, Z.-Q.; Zhu, Y.; Alam, B.; Albrecht, B. J.; Aldossary, A.; Alguire, E.; Andersen, J. H.; Athavale, V.; Barton, D.; Begam, K.; Behn, A.; Bellonzi, N.; Bernard, Y. A.; Berquist, E. J.; Burton, H. G. A.; Carreras, A.; Carter-Fenk, K.; Chakraborty, R.; Chien, A. D.; Closser, K. D.; Cofer-Shabica, V.; Dasgupta, S.; de Wergifosse, M.; Deng, J.; Diedenhofen, M.; Do, H.; Ehlert, S.; Fang, P.-T.; Fatehi, S.; Feng, Q.; Friedhoff, T.; Gayvert, J.; Ge, Q.; Gidofalvi, G.; Goldey, M.; Gomes, J.; González-Espinoza, C. E.; Gulania, S.; Gunina, A. O.; Hanson-Heine, M. W. D.; Harbach, P. H. P.; Hauser, A.; Herbst, M. F.; Hernández Vera, M.; Hodecker, M.; Holden, Z. C.; Houck, S.; Huang, X.; Hui, K.; Huynh, B. C.; Ivanov, M.; Jász, Á.; Ji, H.; Jiang, H.; Kaduk, B.; Kähler, S.; Khistyayev, K.; Kim, J.; Kis, G.; Klunzinger, P.; Koczor-Benda, Z.; Koh, J. H.; Kosenkov, D.; Koulias, L.; Kowalczyk, T.; Krauter, C. M.; Kue, K.; Kunitsa, A.; Kus, T.; Ladjánszki, I.; Landau, A.; Lawler, K. V.; Lefrancois, D.; Lehtola, S.; Li, R. R.; Li, Y.-P.; Liang, J.; Liebenthal, M.; Lin, H.-H.; Lin, Y.-S.; Liu, F.; Liu, K.-Y.; Loipersberger, M.; Luenser, A.; Manjanath, A.; Manohar, P.; Mansoor, E.; Manzer, S. F.; Mao, S.-P.;

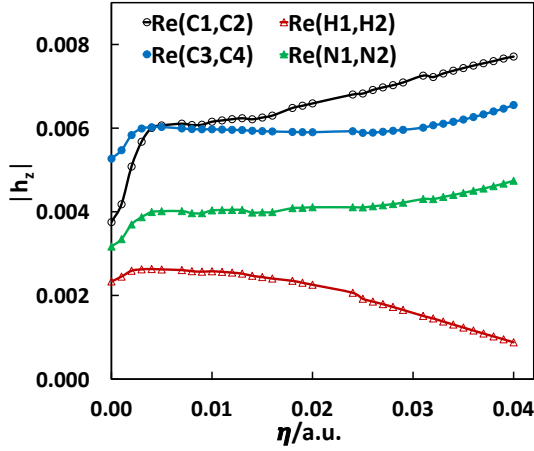
Marenich, A. V.; Markovich, T.; Mason, S.; Maurer, S. A.; McLaughlin, P. F.; Menger, M. F. S. J.; Mewes, J.-M.; Mewes, S. A.; Morgante, P.; Mullinax, J. W.; Oosterbaan, K. J.; Paran, G.; Paul, A. C.; Paul, S. K.; Pavošević, F.; Pei, Z.; Prager, S.; Proynov, E. I.; Rák, Á.; Ramos-Cordoba, E.; Rana, B.; Rask, A. E.; Rettig, A.; Richard, R. M.; Rob, F.; Rossomme, E.; Scheele, T.; Scheurer, M.; Schneider, M.; Sergueev, N.; Sharada, S. M.; Skomorowski, W.; Small, D. W.; Stein, C. J.; Su, Y.-C.; Sundstrom, E. J.; Tao, Z.; Thirman, J.; Tornai, G. J.; Tsuchimochi, T.; Tubman, N. M.; Veccham, S. P.; Vydrov, O.; Wenzel, J.; Witte, J.; Yamada, A.; Yao, K.; Yeganeh, S.; Yost, S. R.; Zech, A.; Zhang, I. Y.; Zhang, X.; Zhang, Y.; Zuev, D.; Aspuru-Guzik, A.; Bell, A. T.; Besley, N. A.; Bravaya, K. B.; Brooks, B. R.; Casanova, D.; Chai, J.-D.; Coriani, S.; Cramer, C. J.; Cserey, G.; DePrince, A. E.; DiStasio, R. A.; Dreuw, A.; Dunietz, B. D.; Furlani, T. R.; Goddard, W. A.; Hammes-Schiffer, S.; Head-Gordon, T.; Hehre, W. J.; Hsu, C.-P.; Jagau, T.-C.; Jung, Y.; Klamt, A.; Kong, J.; Lambrecht, D. S.; Liang, W.; Mayhall, N. J.; McCurdy, C. W.; Neaton, J. B.; Ochsenfeld, C.; Parkhill, J. A.; Peverati, R.; Rassolov, V. A.; Shao, Y.; Slipchenko, L. V.; Stauch, T.; Steele, R. P.; Subotnik, J. E.; Thom, A. J. W.; Tkatchenko, A.; Truhlar, D. G.; Van Voorhis, T.; Wesolowski, T. A.; Whaley, K. B.; Woodcock, H. L.; Zimmerman, P. M.; Faraji, S.; Gill, P. M. W.; Head-Gordon, M.; Herbert, J. M.; Krylov, A. I. Software for the frontiers of quantum chemistry: An overview of developments in the Q-Chem 5 package. *J. Chem. Phys.* **2021**, *155*, 084801.

- (83) Ehara, M.; Kanazawa, Y.; Sommerfeld, T. Low-lying π^* resonances associated with cyano groups: A CAP/SAC-CI study. *Chem. Phys.* **2017**, *482*, 169–177.
- (84) Becke, A. D. Density-functional thermochemistry. III. The role of exact exchange. *J. Chem. Phys.* **1993**, *98*, 5648–5652.
- (85) Stephens, P. J.; Devlin, F. J.; Chabalowski, C. F.; Frisch, M. J. Ab Initio Calculation

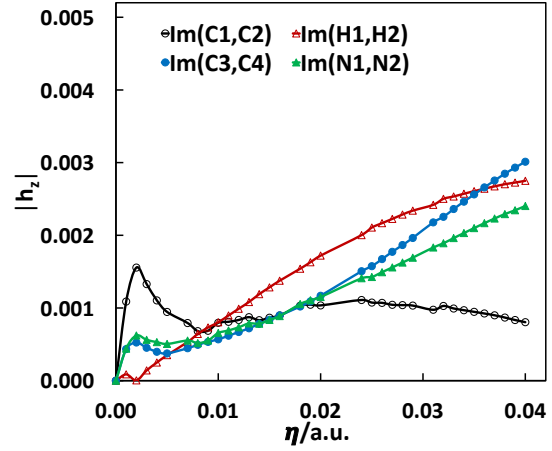
- of Vibrational Absorption and Circular Dichroism Spectra Using Density Functional Force Fields. *J. Phys. Chem.* **1994**, *98*, 11623–11627.
- (86) Dunning, T. H. Gaussian basis sets for use in correlated molecular calculations. I. The atoms boron through neon and hydrogen. *J. Chem. Phys.* **1989**, *90*, 1007–1023.
- (87) Khuseynov, D.; Dixon, A. R.; Dokuchitz, D. J.; Sanov, A. Photochemistry of Fumaronitrile Radical Anion and Its Clusters. *J. Phys. Chem. A* **2014**, *118*, 4510–4518.
- (88) Burrow, P. D.; Howard, A. E.; Johnston, A. R.; Jordan, K. D. Temporary anion states of hydrogen cyanide, methyl cyanide, and methylene dicyanide, selected cyanoethylenes, benzonitrile, and tetracyanoquinodimethane. *J. Phys. Chem.* **1992**, *96*, 7570–7578.

TOC Graphic

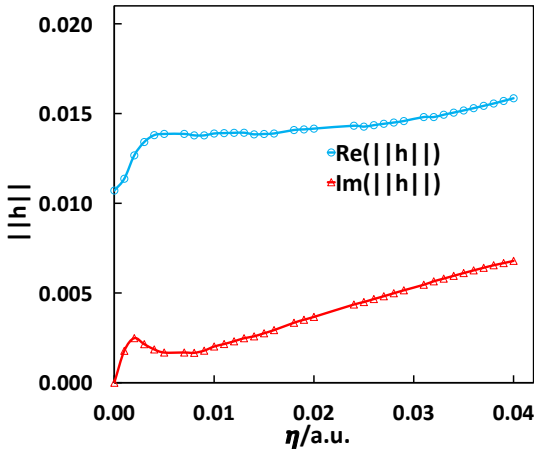




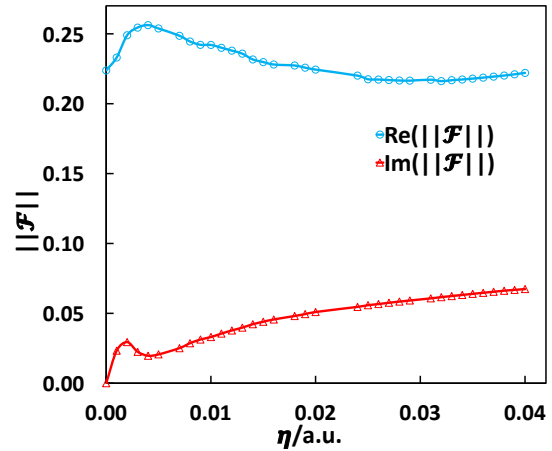
(a) Elements of $\text{Re}(h)$.



(b) Elements of $\text{Im}(h)$.

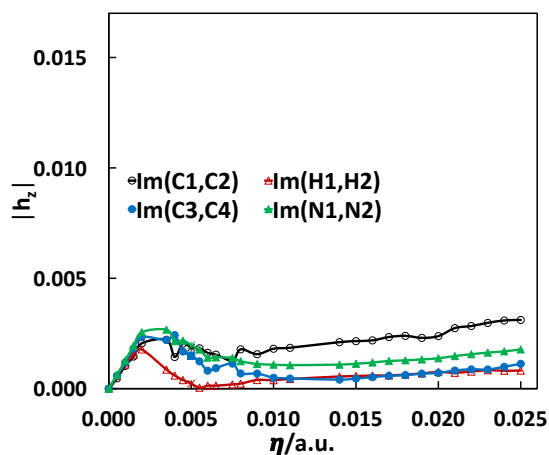
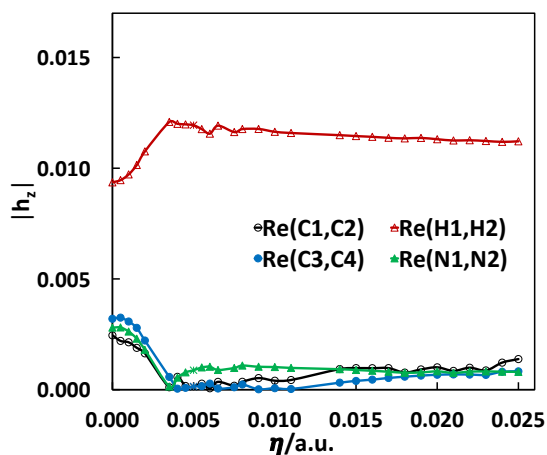
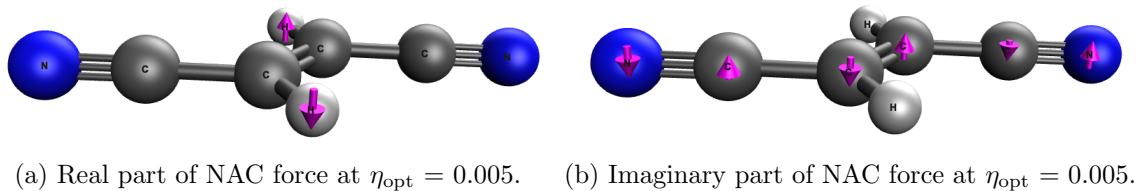


(c) Norms of $\text{Re}(h)$ and $\text{Im}(h)$.



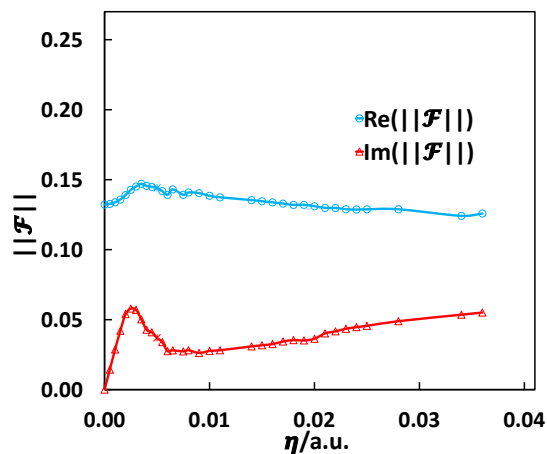
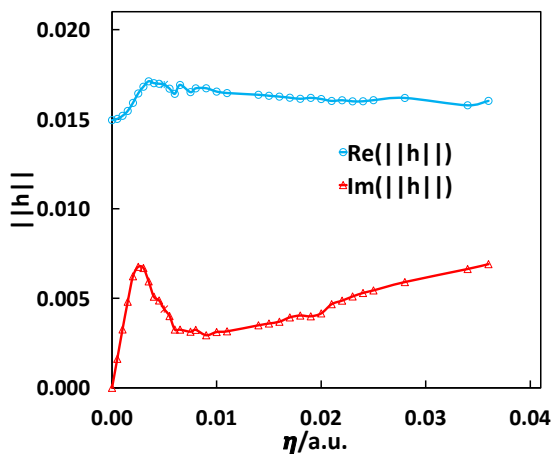
(d) Norms of $\text{Re}(\mathcal{F})$ and $\text{Im}(\mathcal{F})$.

Figure 3: Non-adiabatic coupling force h and derivative coupling \mathcal{F} between the lowest pseudocontinuum state of A_g symmetry and the bound 2B_g state of fumaronitrile anion as a function of CAP strength η computed at the equilibrium structure of the neutral molecule. See Sec. 4 for explanation of the atom labels.



(c) Elements of $\text{Re}(h)$.

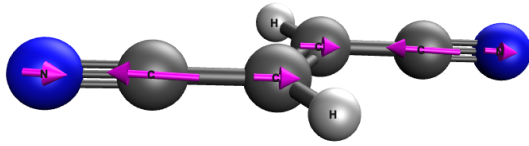
(d) Elements of $\text{Im}(h)$.



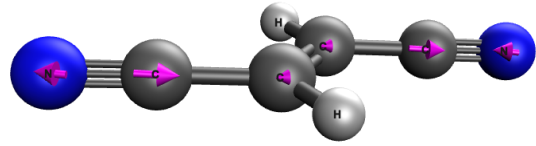
(e) Norms of $\text{Re}(h)$ and $\text{Im}(h)$.

(f) Norms of $\text{Re}(\mathcal{F})$ and $\text{Im}(\mathcal{F})$.

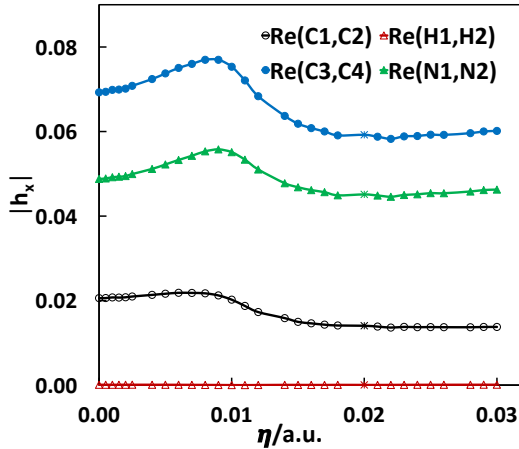
Figure 4: Non-adiabatic coupling force h and derivative coupling \mathcal{F} between the 2A_g resonance and the bound 2B_g state of fumaronitrile anion as a function of CAP strength η computed at the equilibrium structure of the neutral molecule. See Sec. 4 for explanation of the atom labels.



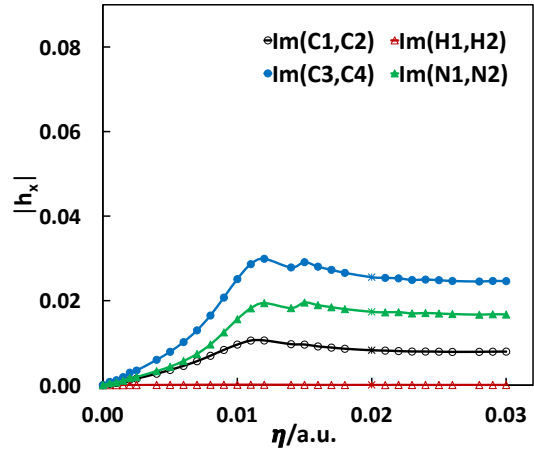
(a) Real part of NAC force at $\eta_{\text{opt}} = 0.02$.



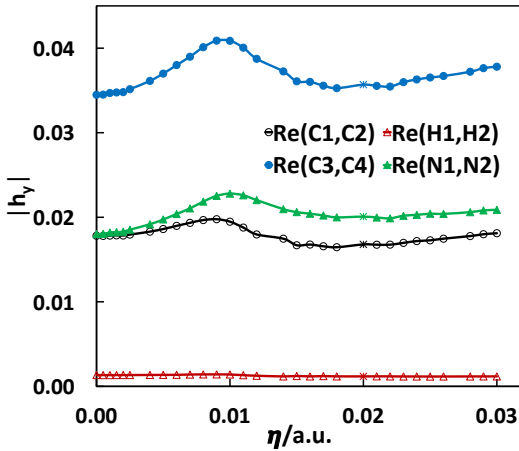
(b) Imaginary part of NAC force at $\eta_{\text{opt}} = 0.02$.



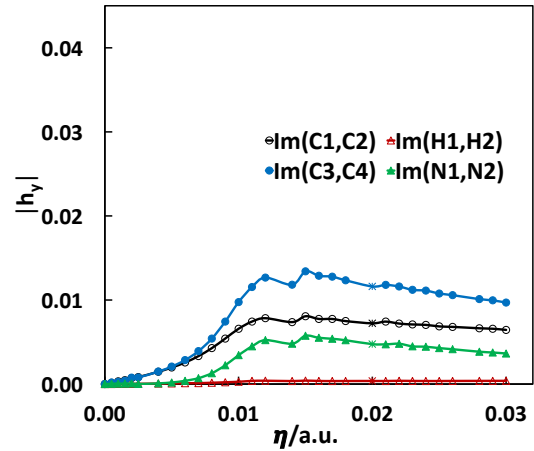
(c) Elements of $\text{Re}(h)$, motion in x direction.



(d) Elements of $\text{Im}(h)$, motion in x direction.

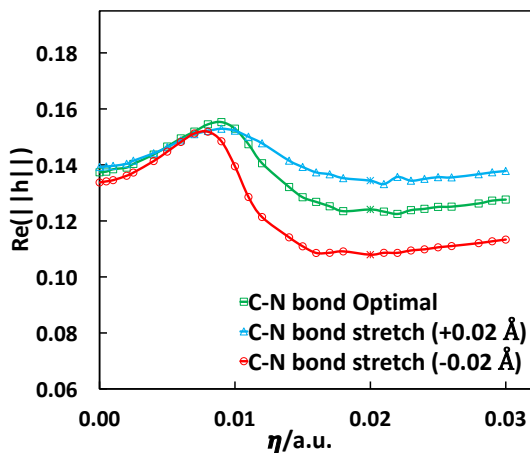


(e) Elements of $\text{Re}(h)$, motion in y direction.

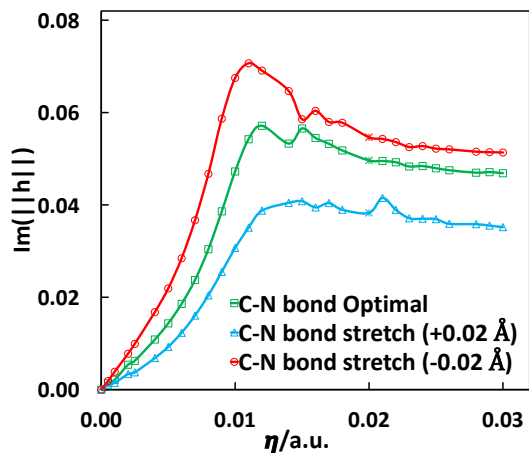


(f) Elements of $\text{Im}(h)$, motion in y direction.

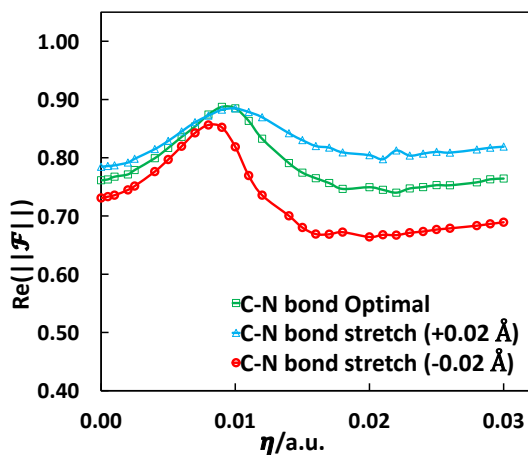
Figure 5: Non-adiabatic coupling force h between the 2A_u resonance and the bound 2B_g state of fumaronitrile anion as a function of CAP strength η computed at the equilibrium structure of the neutral molecule. See Sec. 4 for explanation of the atom labels.



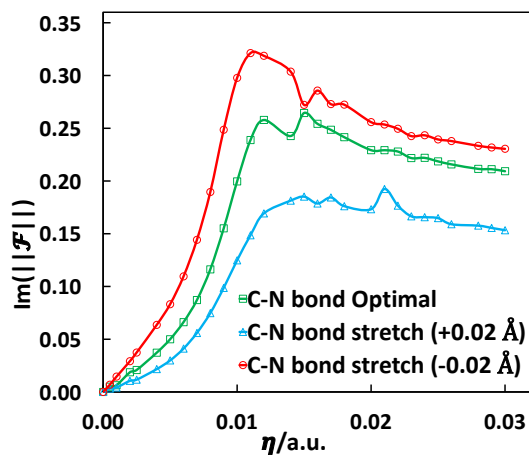
(a) Norm of $\text{Re}(h)$.



(b) Norm of $\text{Im}(h)$.

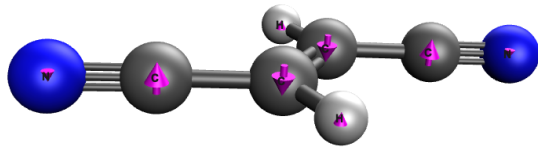


(c) Norm of $\text{Re}(\mathcal{F})$.

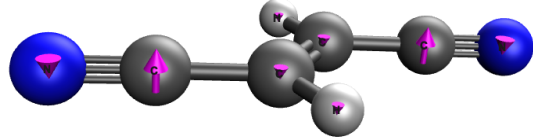


(d) Norm of $\text{Im}(\mathcal{F})$.

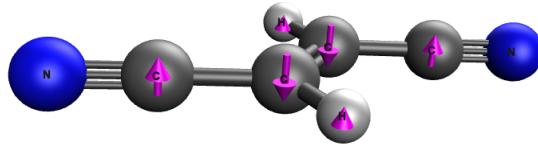
Figure 6: Non-adiabatic coupling force h and derivative coupling \mathcal{F} between the 2A_u resonance and the bound 2B_g state of fumaronitrile anion as a function of CAP strength η at different structures.



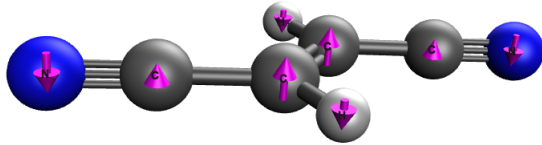
(a) Real part of NAC force at $\eta_{\text{opt}} = 0.005$.



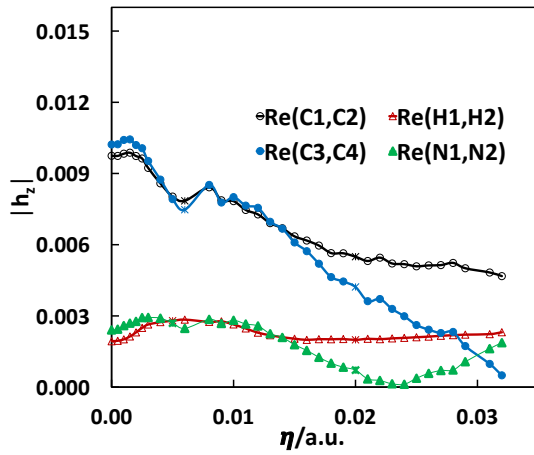
(b) Imaginary part of NAC force at $\eta_{\text{opt}} = 0.005$.



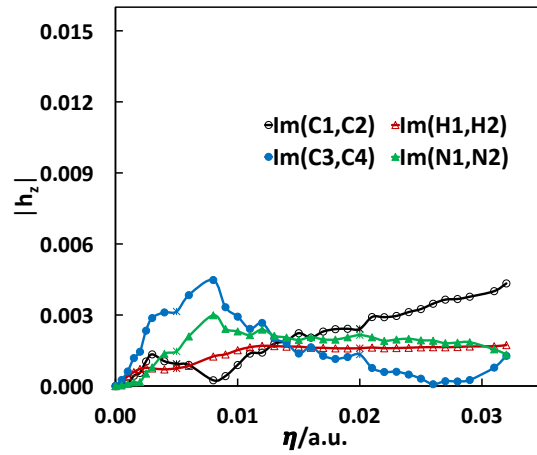
(c) Real part of NAC force at $\eta_{\text{opt}} = 0.02$.



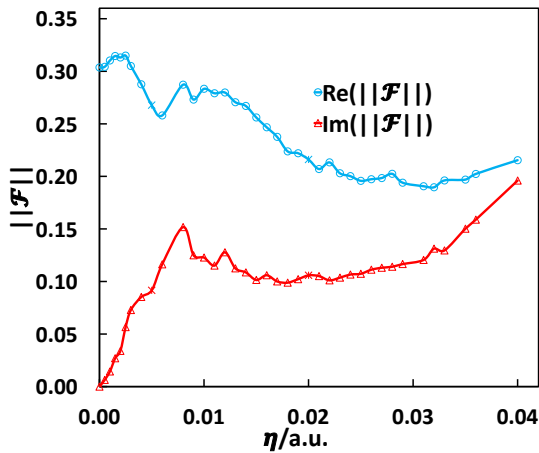
(d) Imaginary part of NAC force at $\eta_{\text{opt}} = 0.02$.



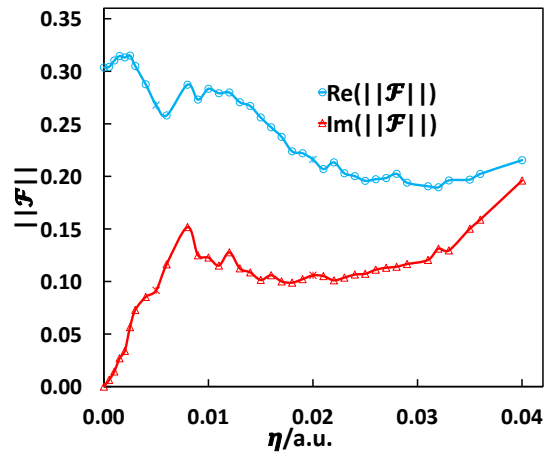
(e) Elements of $\text{Re}(h)$.



(f) Elements of $\text{Im}(h)$.



(g) Norms of $\text{Re}(h)$ and $\text{Im}(h)$.



(h) Norms of $\text{Re}(\mathcal{F})$ and $\text{Im}(\mathcal{F})$.

Figure 7: Non-adiabatic coupling force h and derivative coupling \mathcal{F} between the 2A_g and 2A_u resonances of fumaronitrile anion as a function of CAP strength η computed at the equilibrium structure of the neutral molecule. See Sec. 4 for explanation of the atom labels.